

Article

Experimental and Numerical Analysis of Laterally Loaded Single- and Double-Paddled H-Piles in Clay

Abdelrahman Abouziad  and M. Hesham El Naggar * 

Department of Civil and Environmental Engineering, Western University, London, ON N6A 5B9, Canada; aabouza@uwo.ca

* Correspondence: naggar@uwo.ca

Abstract: An efficient foundation system of single- or double-paddled H-piles (PHPs), which comprises steel H-piles fitted with specially configured steel plates (paddles), is proposed to support sound walls subjected to wind loading. The lateral responses of single-paddled (SPHPs) and double-paddled H-piles (DPHPs) installed in clay is evaluated using a comprehensive assessment of the foundation performance via a full-scale lateral load testing program, alongside extensive three-dimensional (3D) nonlinear finite element (FE) analysis. The comparison between the calculated and measured responses of the PHPs demonstrates that the developed numerical model accurately depicts the response of the PHPs under lateral load. The validated numerical model is then used to evaluate the effect of the soil consistency on the lateral response and capacity of the PHPs. The influence of the paddles' configuration on the lateral response and capacity of the PHPs is also evaluated. Furthermore, the change in the PHP lateral stiffness due to adding a second paddle is also examined. Finally, the influence of the plates on the surrounding soil is investigated by analyzing the formation of the strain field around the pile and evaluating the extent of the soil influence zone at different plate-width-to-pile-flange-width ratios (W_p/W_f). The result of this study indicates that adding plates contributes significantly to the lateral capacity of PHPs in clay and reduces the maximum bending moment. The parametric study reveals that the top 5–6 W_p of the soil have a significant effect on the lateral response of the proposed H-pile. Based on the outcomes of the field tests and numerical analysis, optimal geometrical parameters for paddles are proposed.

Keywords: paddled pile; lateral loading; clay; model tests; three-dimensional (3D) numerical analysis; finite element; design optimization



Citation: Abouziad, A.; El Naggar, M.H. Experimental and Numerical Analysis of Laterally Loaded Single- and Double-Paddled H-Piles in Clay. *Geotechnics* **2023**, *3*, 1324–1345. <https://doi.org/10.3390/geotechnics3040072>

Academic Editors: Md Rajibul Karim, Md. Mizanur Rahman and Khoi Nguyen

Received: 12 October 2023
Revised: 6 December 2023
Accepted: 13 December 2023
Published: 15 December 2023



Copyright: © 2023 by the authors. Licensee MDPI, Basel, Switzerland. This article is an open access article distributed under the terms and conditions of the Creative Commons Attribution (CC BY) license (<https://creativecommons.org/licenses/by/4.0/>).

1. Introduction

Pile foundations are frequently employed in applications where they are subjected to lateral loads due to wind, waves, vehicular traffic, earth pressure, and water pressure [1]. The primary means of supporting lateral loads on piles is via the passive resistance of soil located in front of the pile, as well as the shear resistance of the soil surrounding it. The application of lateral loads on a pile induces stresses within the soil located in front of the pile [2]. As the lateral load magnitude increases, the stress in front of the pile also increases, while the stress in the soil behind the pile decreases. Numerous studies were conducted to analyze the lateral response of piles. Model tests and full-scale tests as well as analytical and numerical investigations have been conducted on individual piles to examine their lateral response and capacity and the state of stress in the adjacent soil.

Matlock and Reese [3] provided generalized analytical solutions for laterally loaded vertical piles. Davisson [4] investigated the effect of combined loading (vertical and lateral loads) on the lateral response of a pile. To compute the pile head deflection due to lateral loads, Broms [5] provided a simplified approach based on the theory of subgrade modulus, in which the soil subgrade modulus is assumed to increase linearly with depth and it is assumed that the soil behaves in a linear elastic manner. To account for the soil nonlinearity,

Matlock [6] and Reese et al. [7] developed the concept of nonlinear p - y curves, which is widely used to obtain the lateral response of a pile subjected to lateral loading. The p - y curve is based on the modulus subgrade reaction approach developed by Winkler [8], in which the soil around the pile is replaced by a series of infinitely closely spaced independent springs. The p - y curves represent the soil reaction (p) to pile deflection (y) at different elevations along the pile. The p - y curves are obtained via the analysis of a large number of laterally loaded piles (fully embedded and partially embedded piles), and numerous laboratory and full-scale load tests were used to validate the method [9].

The three-dimensional (3D) finite element method (FEM) allows for consideration of the actual geometry of the piles as well as the continuity of soil and its variability along the pile shaft. Furthermore, it enables simulating the field's actual combined loading conditions. In addition, the FEM can establish the pile and soil responses at individual nodes and elements along the pile shaft, which can be used for comparison with the p - y curve [10]. Several studies utilized the FEM to evaluate the lateral response of a single pile under a cyclic load [11], dynamic and static lateral load [11], monotonic lateral load [12], cyclic load on a driven pile [13], monotonic lateral load in soft clay [14], and cyclic lateral load in undrained clay [15].

Different foundation systems have been utilized to provide support for laterally loaded superstructures. Drilled shafts, which are also referred to as bored piles or cast-in-situ piles, are frequently employed to support lateral loads owing to their large load-bearing capacity and adaptability to diverse soil conditions. Driven piles, such as precast concrete piles, steel piles, and timber piles, are also frequently utilized as a foundation. The utilization of driven piles presents the benefit of expedited installation and can be applied across diverse soil conditions [16]. Compared to standard impact driving, vibratory driving provides several benefits, including quicker installation rates (often three to four times faster), less noise [17] and vibration, and simpler corrections in the event of installation-related misplacements or misalignments [18]. However, vibratory-driven piles exhibited a lower load capacity in comparison to impact-driven or jacked piles according to [19] and tend to experience greater deformation under cyclic lateral loading in comparison to impact-driven piles [20,21]. In addition, piles installed employing vibratory driving usually have small cross-sections to facilitate installation employing relatively small equipment. Although cost-effective, it is important to note that these piles being used as sound wall foundations are prone to excessive lateral displacement due to the relatively high wind load. Therefore, modifications to their cross-section or improvement of the adjacent soil may be necessary to enhance their performance under lateral loading and increase their lateral capacity. The current methods used in practice include improving the soil in the vicinity, modifying the pile dimensions, and utilizing inclined piles.

In response to the market demand for an improved foundation system, the concept of paddled H-piles has emerged. This innovative design offers several advantages, including enhanced lateral load resistance and a reduced construction time [22]. The use of paddled H-piles can provide a viable alternative for supporting laterally loaded structures. Previous studies have investigated the effect of increasing the cross-section of piles on their lateral behaviour. The effectiveness of adding plates to piles (i.e., finned piles) in enhancing their lateral capacity has been proved adequate in silica sand [23]; saturated sand [24]; sand [25]; two sand sites [26]; and clay [18]. The investigations of the lateral performance of finned piles can be classified into four distinct categories: (1) laboratory small-scale tests [27–30]; (2) full-scale field tests in clay [22], sand [26,31], and alluvial sandy silt [32]; (3) centrifuge models [28]; and (4) numerical analysis using 3D (PFC3D) software [24], the PLAXIS program [29,30], and Abaqus [33,34]. The main emphasis of the published studies on finned piles has been on improving the lateral load capacity of the pipe piles commonly utilized in offshore wind turbine foundations. These piles typically have large diameters and a large embedment depth and are installed using conventional driving methods. Most of these studies have focused on the arrangement of the fins, and their number, shape, and size. However, alternative types of piles, such as H-piles, are considered more suitable for other

infrastructure projects like sound walls. Pile installation employing vibratory hammers can affect the mechanical characteristics of the adjacent soil and consequently affect the lateral response of piles. In addition, piles supporting sound walls are primarily subjected to lateral loads with minimal axial loads; correspondingly, the piles will have a small cross-section and small embedded length. Hence, their behaviour will be vastly different from the large offshore piles that are installed using conventional driving hammers.

This study investigates paddled H-piles (PHPs) installed using a vibratory hammer in cohesive soil for sound wall applications. The study involved two phases: phase 1, which involved the installation and testing of full-scale double-paddle H-piles; and phase 2, which involved 3D nonlinear finite element analysis of single- and double-PHPs subjected to lateral loads in clay soil. The computer program PLAXIS 3D was used to develop the finite element model to simulate the response of the tested piles. The numerical model's reliability and accuracy were ensured via a validation process, which involved comparing its results with the data obtained from the field tests. Subsequently, the validated finite element model was employed to conduct a comprehensive parametric analysis with the objective of evaluating the effectiveness of single- and double-paddled H-piles in resisting lateral loads, specifically the influence of the number and paddle dimensions (width and length) on the lateral stiffness of the PHPs. This parametric analysis yielded significant insights into the influence of the PHPs on the surrounding soil. The findings of this study have the potential to establish design guidelines for PHPs, as well as guidance for the enhancement of engineering techniques concerning foundation systems subjected to lateral loads.

2. Site Investigation Program

The full-scale experiments were conducted at the test facility at the Environmental Sciences Western Field Station situated at 22,312 Wonderland Road North, London. A geotechnical investigation was conducted for the test site involving nine boreholes conducted in 2008 and two boreholes conducted in 2012. In addition, [9,22] conducted a laboratory test program in compliance with ASTM standards on soil samples retrieved from an additional borehole in the designated test area. The laboratory testing program encompassed determining the soil moisture content, Atterberg limits, and grain size distribution. In addition, [35,36] conducted undrained unconsolidated triaxial tests on undisturbed samples retrieved from the site, according to ASTM (D 2850-95), to determine the soil's undrained shear strength values. The undrained shear strength of the soil was further investigated using the SPT field value [22,35,36]. The site investigation along with the laboratory tests indicated that the site consists of predominantly cohesive soil (A-6 clayey soil, AASHTO soil classification). The soil profile comprised a layer of light brown silty topsoil of 0.15 m thickness with some sand, overlaying a layer of stiff lean clay with sand of 0.75 m thickness, which lies over a layer of stiff lean clay with sand. A layer of light gray sandy lean clay appears below a depth of 4.6 m. The soil undrained shear strength (S_u) values were measured and ranged between 60 and 110 kN/m², with an average of 97 kN/m². Table 1 provides an overview of the field and laboratory tests conducted, as well as the idealized soil profile based on the data obtained from these tests. The Standard Penetration Test (SPT) N values were documented along the depth. Soil samples were obtained at intervals of 150 mm, and blow counts of 17, 11, 22, and 15 were recorded corresponding to sample depths of 0.3–0.9 m, 1.5–2.1 m, 2.6–3.3 m, and 4.6–5.2 m, respectively. This information is utilized in a subsequent finite element (FE) model.

Table 1. Summary of and laboratory tests and the idealized soil profile.

Laboratory Test Data				Idealized Soil Profile		
Soil Type	Depth of the Sample (m)	PI (%)	LL (%)	Depth (m)	Unite Wt. (KN/m ³)	S_u (KN/m ²)
Topsoil	-	-	-	-	-	-
Stiff brown lean clay with sand (1.6% Gravel, 17.8% Sand, 63.7% Silt, and 16.9% clay)	0.7–0.9	13	32	0–0.9	19	110

Table 1. Cont.

Laboratory Test Data				Idealized Soil Profile		
Soil Type	Depth of the Sample (m)	PI (%)	LL (%)	Depth (m)	Unite Wt. (KN/m ³)	S _u (KN/m ²)
Stiff gray lean clay (0.8% Gravel, 11.7% Sand, 64.7% Silt, and 22.8% clay)	0.9–1.2	17	35	0.9–2.0	21	60
Stiff gray lean clay with Sand (9.1% Gravel, 11.4% Sand, 48.5% Silt, and 31% clay)	2.2–2.6	12	26	2.0–4.7	21.5	125
Light gray sandy lean clay (45.1% Sand)	4.6–5.2	7	21	4.7–7.0	20	95

3. Experimental Program

A field-testing program was executed, which involved lateral loading of W200 × 36 steel H-piles with an embedded length of 3.5 m and a protruding (stickup) length of 1.35 m [18,22]. Lateral load tests were conducted to evaluate the pile's lateral load capacity under varying load conditions. Three types of novel piles were tested: single-paddled H-piles (SPHPs), double-paddled H-piles (DHPs), and noded single-paddled H-piles (NSPHPs). In addition, the performance of conventional drilled shafts (DS) and plain H-piles (PPs) was evaluated and compared to the novel piles. Novel piles were manufactured by welding 950 × 420 × 9 mm paddle-shaped steel plates to one flange for the SPHPs and two flanges for DHPs of the H-pile. A total of 8 piles were subjected to monotonic lateral loads: two SPHPs (denoted as SP-03 and SP-04), two NSPHPs (denoted as SN-03 and SN-04), two drilled shafts (denoted as DS-01 and DS-02), and two PPs (denoted as PP-01 and PP-02). Each pile was instrumented with C2A-06-250LW-120 foil strain gauges along its length at nine levels to measure the bending moments. To ensure the functionality of the strain gauges, three layers of protection were applied to the strain gauges and wires. Figure 1 shows the dimensions of the plate and the nodes. In this study, the FE model is validated using the load–displacement curves of SPHP-03, SPHP-04, PP-01, and PP-02.

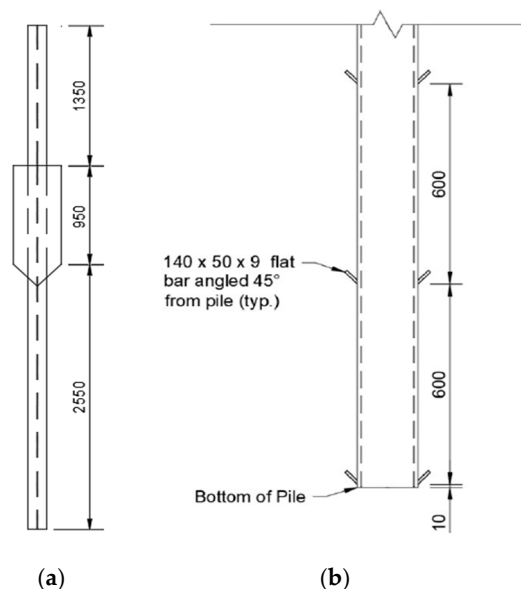


Figure 1. Novel pile profile; (a) plate dimensions and location in the test; (b) location, dimension, and orientation of nodes on the pile. (Dimensions in mm).

Vibratory driving was utilized to install the piles using an excavator-mounted 320 vibro hammer. The insulation quality and driving time of each pile were recorded. The records demonstrated that the average driving time of the steel piles was 3–4.4 times faster than the installation of the DS, including the time for the drilling, pouring of concrete, and placing of the steel reinforcement only. In accordance with the prescribed methodology outlined in ASTM D3966 method 6.4, lateral load tests were conducted on tested piles to ascertain their

response under gradually increasing lateral load. To facilitate simultaneous testing of both piles, an RRH 1006 Enerpac double-acting hydraulic jack(s) with a capacity of 1100 KN was positioned between the two piles, the application of load in increments equivalent to 5% of the anticipated failure load. The load was applied at a height of 1.25 m above the ground elevation [37]. The lateral deflection was measured using three 100 mm stork potentiometers with 0.1 mm accuracy, and data were collected every 5 s using a 7000 series Sciometric data acquisition system. All components of the test (i.e., stork potentiometers and hydraulic jack) were leveled before conducting the test; Figure 2. Comprehensive details of the soil properties at the test site, testing setup, and procedure are available elsewhere [22].



Figure 2. Lateral load test setup for two piles tested simultaneously.

3.1. Lateral Monotonic Test Result

The structural performance of the test piles subjected to lateral loads was assessed. Two types of piles were investigated: plain H-piles (PPs) and single-paddled H-pile (SPHPs). The loading was specifically applied along the weak axis of the piles, which is defined as the axis possessing the lower moment of inertia. Furthermore, the load was applied to the unpaddled flange of the piles. The lateral load test was conducted on two plain pile specimens (PP-01 and PP-02) and two PHP specimens (SPHP-03 and SPHP-04).

3.2. Load Displacement Curve

Figure 3 displays the horizontal load–displacement curves of the PHP test piles. Figure 3 also presents the load–displacement curves obtained from the finite element analysis, as will be discussed later. Via the field tests, the values of the ultimate capacity for SPHP-03 and SPHP-04 were determined as 42 KN and 42.5 KN, respectively. These capacities correspond to lateral displacements of 19.13 mm and 9.35 mm, respectively. Notably, the SPHP-03 test deviated from the SPHP-04 test, showing a much lower lateral resistance. The weaker mechanical response and reduced stiffness are ascribed to suboptimal installation practices, which were observed during installation, leading to significant soil disturbance during the installation process, as highlighted by [22].

Figure 4 presents the load–displacement curves of the plain piles PP-01 and PP-02. The ultimate lateral capacity of PP-02 and PP-01 was 46.5 KN, which corresponded to lateral displacements of 18.5 mm and 26.6 mm, respectively. The higher lateral rigidity exhibited by PP-02 is attributed to the inherent heterogeneity of the soil composition.

Figure 5 depicts the envelope behaviour of the load–displacement curves obtained from the field tests of the two posts SPHP-04 and PP-02. The expected load–displacement characteristics of a laterally loaded pile can be dissected into three distinct phases: an initial linear behaviour, followed by a nonlinear response, demonstrating a propensity

for plasticity. The final stage is distinguished by the occurrence of complete slippage along the lateral surface of the pile and the complete adaptability of the supporting soil, which is indicated by the linear segment observed at the concluding portion of the load–displacement curve. The third stage is not shown in Figure 5, indicating that the load did not plateau, i.e., did not reach complete failure, which is characterized by a large increase in displacement with a small increase in load. This is a result of the relatively low applied load because of the limitation of the loading setup.

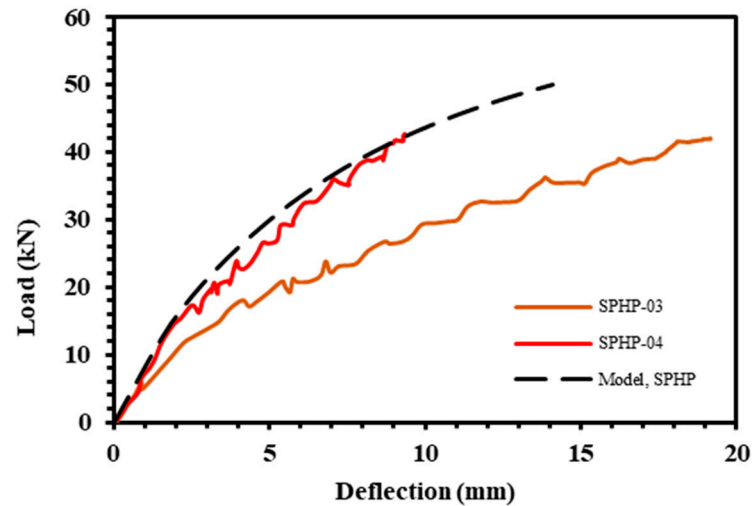


Figure 3. Comparison of load–displacement curves obtained from the calibrated FEM and pile load tests SPHP-03 and SPHP-04.

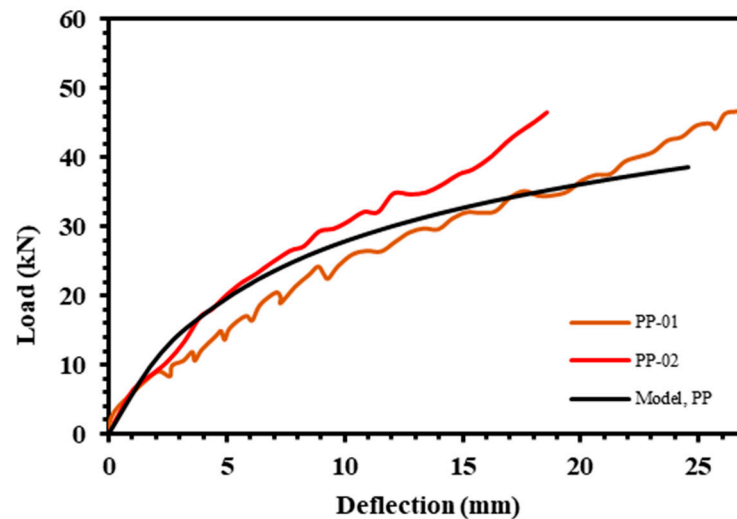


Figure 4. Comparison of load–displacement curves obtained from the calibrated FEM and pile load tests for the PP-01 and PP-02 innovative post.

Similar behaviour was observed by Drbe and El Naggar [35] in their study of laterally loaded micropiles, and a similar pattern was reported by [38] with the additional observation of heaving and gap opening during the second phase and a linear segment at the last stage. This three-segment behaviour can be attributed to the deformation mechanism: global and local [26]. As a result of the imposed load at the pile head, the pile and surrounding soil move as a single unit, constituting the global mechanism. The global mechanism culminates with the pile shaft detaching from the soil behind the applied force, creating a gap, and as the applied load increases, local failure occurs. Comparing the performance

of both sets of tested piles (PPs and PHPs), it was determined that the PHPs exhibited a generally stiffer response than the PPs.

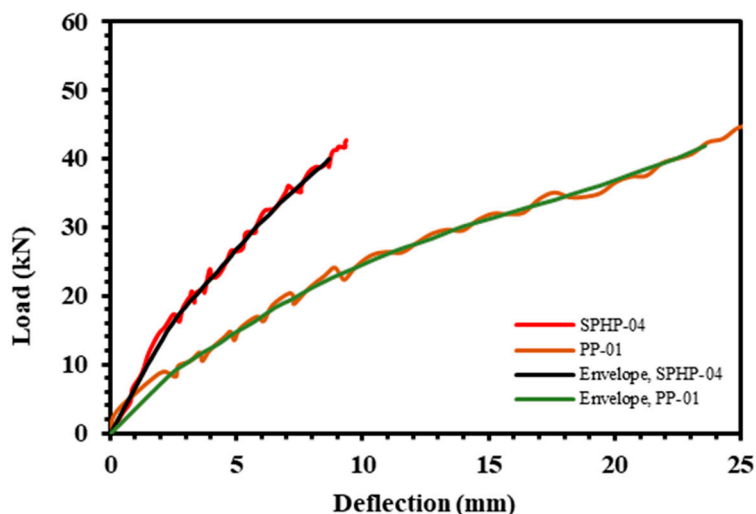


Figure 5. Load–displacement curve and envelope load–displacement curve for SP-04 and PP-02.

Failure Mechanism

The ultimate lateral capacity of the pile depends on the type of pile (long or short) and the soil. Brinch Hansen’s method [39] and Broms’ method [5] use soil resistance and equations of static equilibrium to solve for the ultimate lateral load. Broms’ method can be applied to both long and short piles, whereas Brinch Hansen’s method is specifically applicable to short piles. However, in practice, the design of laterally loaded piles often focuses on acceptable deflection rather than ultimate soil resistance [40]. This approach recognizes that the primary concern is to ensure that the lateral deflection of the pile remains within acceptable limits, considering factors such as the structural requirements, serviceability, and the desired performance of the pile foundation system. The determination of an acceptable lateral load in relation to an acceptable deflection is commonly derived from a load–deflection curve that is developed via the analysis of the lateral pile load. Table 2 illustrates the failure criteria based on the pile’s head lateral displacement provided by [41–43] and the corresponding lateral load determined based on the field test data. As anticipated, the lateral capacity of the piles demonstrates an upward trend as the tolerance for lateral deflection increases.

Table 2. Ultimate lateral capacity for innovative posts.

Reference	Criteria Load at	Ultimate Design Lateral Capacity (KN)			
		PP-01	PP-02	SP-03	SP-04
(McNulty, 1956) [41]	6.25 mm	18	23	21	32
(Walker & Cox, 1966) [42]	13.0 mm	29	35	33	-
(New York City, 1981) [44]	25.0 mm	45	-	-	-

4. Numerical Model

The three-dimensional finite element software PLAXIS 3D was utilized to conduct the numerical investigation in order to account for the complexity of the pile geometry and loading system, as well as the soil nonlinearity [43]. The numerical model accurately represented the tested PHPs, including their geometry and material properties, as well as the surrounding soil medium and its properties. The local soil stratigraphy was incorporated using the data obtained from the boreholes. To replicate the exact geometry of the test piles, the volume of the piles was accurately represented in the numerical model. Once

the entire geometry model was defined and the initial properties were assigned, a finite element mesh was generated. To ensure accurate simulation of deformation and geometric curvatures, 10-node tetrahedral elements were employed to discretize the soil domain, enabling second-order displacement interpolation.

4.1. Pile Modelling

The steel pile and soil layers were represented as discrete volume elements comprising 10-node tetrahedral elements. This methodology facilitates the utilization of second-order interpolation techniques for accurately estimating the displacements. The steel pile was simulated using nonporous elastic–perfectly plastic material with unit weight (γ_{sat}) and the stiffness parameters Young’s modulus (E) and Poisson’s ratio (ν). The soil–pile interaction was simulated using 15 noded interface elements, which is based on Newton–Cotes integration. The roughness of the interaction is modeled by setting the strength reduction factor (R_{inter}) equal to 2/3 to allow for a reduction in the friction angle and the cohesion of the soil around the pile [29,33,34,45]. The strength parameter reduction was utilized in the slippage phase. A virtual thickness, serving as an abstract measure of the interface, dictates the extent of elastic deformation generated and was assigned a default value of 0.1.

4.2. Soil Modelling

Proper consideration of the soil’s nonlinear response to lateral stress is crucial when analyzing the soil response when subjected to external loads. To properly account for soil nonlinearity, the widely used linear elastic–perfectly plastic (Mohr–Coulomb, MC) model was used to simulate the soil behaviour under a lateral load. This model allows for practical evaluation and the use of critical soil parameters such as the soil’s undrained shear strength, Poisson’s ratio, cohesion, friction angle, and dilatancy angle, making it a popular choice for geotechnical problems. The linear elastic perfectly–plastic soil model employs Hooke’s law to establish the relationship between the rates of stress and elastic strain. The stress–strain relationship progresses linearly until reaching a point of yielding, after which it transitions into a yield “plateau”. Subsequently, the stress–strain relationship is governed by the Mohr–Coulomb failure criterion for the perfectly plastic part of the model. The soil stiffness is determined by two key factors: the soil modulus of elasticity and Poisson’s ratio. Furthermore, the strength parameters of the Mohr–Coulomb model include the cohesiveness, friction angle, and dilatancy angle. The soil profile was divided into four layers, and the mechanical and strength parameters were defined based on the averaged values.

The undrained condition was adopted in the analysis to account for the soil’s low permeability. Since no volume change occurs for undrained loading of saturated cohesive soil (i.e., $\phi = 0$ condition), the undrained Poisson’s ratio (ν_u) was set equal to 0.499 [46] The undrained Young’s modulus (E_u) was evaluated employing the empirical correlations with the SPT N value provided by the NRC of Canada. Table 3 summarizes the correlation of S_u and E_u with the SPT N value.

Flaate [47] studied the effect of pile driving on the strength and deformation properties of clay. The results showed that during the driving process of a pile into clay, a significant remolding phenomenon occurs in a zone approximately 10 to 15 cm from the surface of the pile. Beyond this zone, there is also a reduction in strength and changes in the stress–strain properties. The extent of this remolding effect depends on various factors such as the clay properties, driving method, pile dimensions, and pile density. Notably, when considering a pile group, the remolding effect tends to be more pronounced compared to a single pile. Randolph [48] stated that conventional driving of piles into clay causes a remolded zone around the pile with a reduced strength as low as 1/5 of the native clay peak strength. Thus, a weaker soil zone with a remolded S_u equal to 1/6 of the peak S_u was modeled around the pile to account for the disturbed and compressed soil due to the pile’s installation process (vibratory-driven piles). The used strength reduction factor (1/6) resulted in good agreement with the measured field data. The suggested increase in the

reduction factor proposed by Randolph is attributed to the relatively larger width of the prestressed high-performance (PHP) pile.

Table 3. Correlation of undrained modulus of elasticity and undrained shear strength.

Source	Soil Type	Correlations	Layer Number			
			1	2	3	4
			N N60	17 14	11 11	22 20
Undrained Shear Strength (KPa)						
	Previous measured data		110	60	125	95
Stroud (1974) [49]	Clay, $I_p < 20$	$S_u = 6-7 N$	111	72	143	98
Sivrilaya and Togral (2002) [50]	Fine-grained soil	$S_u = 6.18 N60$	87	56	111	93
Terzaghi and Peck (1967) [51]	Fine-grained soil	$S_u = 6.25 N$	106	69	138	94
Kumar (2016) [52]	Cohesion soil, $N = 2-30$	$S_u = -2.2049 + 6.484 N$	108	69	140	95
Undrained modulus of elasticity (MPa)						
	Soft sensitive clay	$E_s = 0.5 S_u$	55	30	62.5	47.5
NRC of Canada (1975) [53]	Fine to stiff clay	$E_s = 1 S_u$	110	60	125	95
	Very stiff clay	$E_s = 1.5 S_u$	165	90	187.5	142.5
Bjerrum (1972) [54]	Clay, $I_p < 30$, or stiff	$E_s = (0.5 \text{ to } 1.5) S_u$				
Bowles (1982) [55]						

In order to accurately determine the undrained Young’s modulus at a specific site, a combination of trial-and-error methodology, field data analysis, and comparison with finite element (FE) models is usually employed. Suitable correlations, which effectively define the undrained Young’s modulus, were carefully selected. Notably, the correlations proposed by [49,51,56] were utilized, leading to a reasonably estimated range for the undrained shear strength (S_u) based on the Standard Penetration Test (SPT) data as determined by [22]. Additionally, [52] established empirical correlations for the undrained shear strength of various soil types by incorporating data from [57] and employing random number generation techniques. Remarkably, their findings exhibited strong agreement with the previously measured data. Table 4 presents a detailed overview of the mechanical and strength parameters of the soil established from those correlations and employed in the 3D FE models.

Table 4. Material properties for PLAXIS 3D soil model.

Parameters		Pile	Soil Profile			
			Layer 1	Layer 2	Layer 3	Layer 4
General	Unit					
Material Model		Linear elastic				
Drainage Type		Non-porous				
γ_{unsat}	(kN/m ³)	78.5	19	21	21.5	20
Soil Properties						
ν	-	0.3		0.499		
S_u (Field Data)	(kN/m ²)	-	110	60	125	95
E_u (NRC,1975)	(MPa)	2×108	110	60	125	95
			Disturbed Zone			
S_u	(kN/m ²)	-	18	10	21	16
E_u	(MPa)	-	9.167	5.000	10.417	7.917

4.3. Boundary Conditions and Mesh Refinement

In order to mitigate the influence of the boundary conditions on the behaviour of the soil–structure system within the numerical simulation, the model boundaries were positioned at a distance exceeding 10 times the width (B) of the PHP. The finite element (FE) model dimensions were 10 m by 7 m to ensure the minimal impact of the boundaries on the calculated response of the test piles. The PLAXIS 3D standard boundary conditions were applied to the model, which is a normal fixity at vertical boundaries with their normal vector in the X-direction, Y–Z plane ($U_x = 0$, and $U_y = U_z = \text{free}$), and Y-direction ($U_y = 0$ and $U_x = U_z = \text{free}$), as shown in Figure 6. A full fixity was applied to the bottom of the model ($U_x = U_y = U_z = 0$), while free boundary conditions, in all directions, were considered for the ground surface. A comprehensive study was undertaken to explore the convergence properties of different mesh sizes and coarseness parameters. Using coarseness factors of 0.25, 0.5, and 0.1 for the outer soil, inner soil (influenced zone), and the pile, respectively, in conjunction with the utilization of a moderately distributed mesh size, satisfactory alignment with the experimental results was achieved. Figure 6 presents the representative three-dimensional finite element mesh employed to evaluate the performance of the PHPs when subjected to lateral loading.

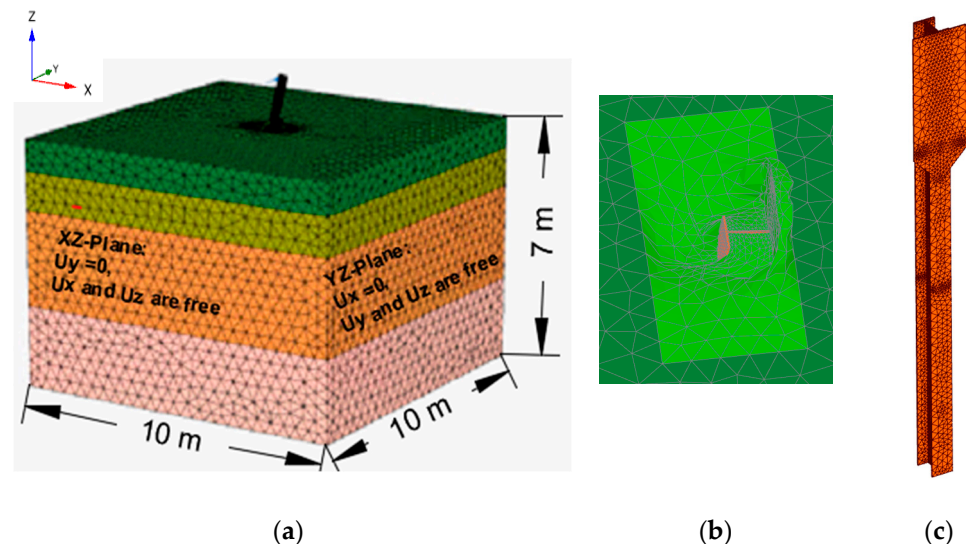


Figure 6. FE model: (a) 3D mesh; (b) soil movement around pile head; and (c) pile geometry.

In order to refine the accuracy of the FE model, field tests of the plain pile were utilized as a means of calibration. Subsequently, the model was validated by comparing its predicted outcomes with the field test data obtained from the PHPs. The satisfactory agreement between the calculated and measured values is depicted in Figure 3, indicating the model's reliability and agreement with observed results, with an exact match for the linear region, the first 1.5 mm of lateral deflection (i.e., soil elastic behaviour is well simulated). Meanwhile, for the load range of 10 kN to 45 kN, the 3D FE results indicate a slightly stiffer reaction of the single-paddled pile than the corresponding field results. In general, the numerical model results are in good agreement between both results up to the maximum applied lateral load.

5. Parametric Study

The lateral capacity of the piles is defined as the load applied at the pile head corresponding to a certain pile head lateral deflection. Accordingly, the available failure criteria based on the pile head lateral displacements are considered herein. In this study, the serviceability limit state (SLS) is determined by [41]'s standards of lateral displacement = 6.25 mm, whereas the ultimate limit state is determined by [44]'s criteria of 25 mm. The performance of the H-pile with a single plate welded in the opposite direction to the load (single PHP)

is compared to the performance of a double PHP. In addition, the influence of the clay consistency (i.e., soft clay and stiff clay) is studied. The effect of the plate width and length on the single-paddled and the double-paddled innovative post-lateral capacity is evaluated. Furthermore, the effect of the paddles on the surrounding soil is investigated. This study considered W200 × 36 steel H-piles and a paddle with the original dimensions of the test piles (i.e., 950 × 420 × 9 mm).

5.1. Effect of Clay Consistency

The effect of the clay consistency on the lateral response of the PHPs is assessed in this section. Table 5 shows the soil parameters used for this parametric study. The values were derived from the SPT N values; the undrained Young’s modulus (E_u) and undrained shear strength were evaluated using the correlation provided by [52] and [53], respectively, as shown in Table 5.

Table 5. Material properties for parametric study.

Soil Properties				
Consistency	N	S_u (KPa)	E_u (KPa)	γ_{unsat}
Soft	3	17	8624	17
Medium	6	37	36,699	18
Stiff	12	76	75,603	19
Very stiff	24	153	230,117	20
Hard	35	225	337,103	22

Figure 7 presents the lateral load for piles installed in soil with different values of undrained shear strength considering the SLS (6.25 mm pile head displacement) and ULS (25 mm pile head displacement) failure criteria. As expected, the lateral capacity of the PHP decreases as the S_u value decreases; however, the rate of change differed slightly depending on the failure criteria. For a lateral displacement of 6.25 mm, the capacity of the DPHP decreases by 20%, 40%, 37%, and 52% for $S_u = 153, 76, 37,$ and 17 kPa, respectively, compared to the capacity for $S_u = 225$ kPa. The incremental decrease in the capacity of the SPHP is comparable to that of the DPHP.

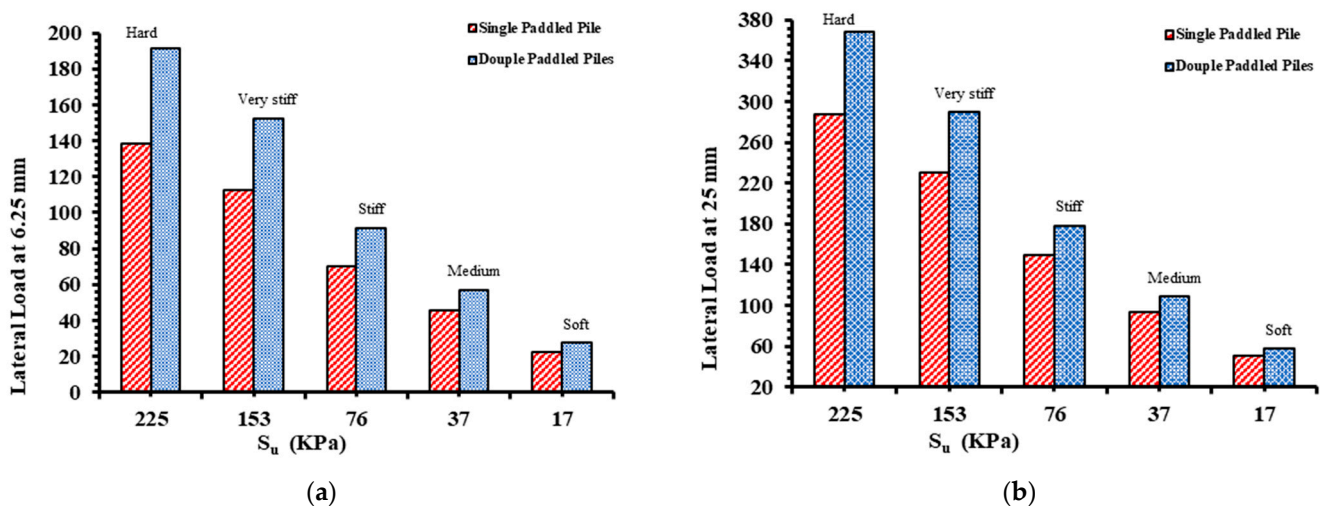


Figure 7. Relationship between lateral load at lateral deflection of (a) 6.25 mm and (b) 25 mm and soil consistency.

In general, the capacity of the paddled pile considering the ULS is less influenced by the decrease in the S_u value, with a loss in capacity of 38%, 39%, and 47% for undrained

shear strength values of 76, 37, and 17 (KPa), respectively. However, the lateral capacity decreased at a greater rate for very stiff clay than for the 6.25 mm failure criterion.

The performance of the innovative posts was also evaluated using a load efficiency, η_L , which is defined as the increase in the lateral stiffness of the pile at a given lateral load compared to a corresponding plain pile.

$$\eta_L = \frac{H_{PHp} - H_{PP}}{H_P} \tag{1}$$

where H_{PHp} and H_{pp} are the lateral loads corresponding to the lateral head displacement for the paddled pile and plain pile, respectively.

Figure 8 presents the load efficiency curve, which indicates the variation in the post-lateral load with the consistency of the clay represented in the form of the Standard Penetration (SPT) N value. It is clear that η_L increases as the SPT N value increases and with an increase in the soil–pile contact area, i.e., stiffening the pile with one or two plates contributes significantly to the stiffness of the foundation system and can provide from 28% up to 74% more rigidity (considering the ULS) than the corresponding plain pile. As expected, the double-paddled piles exhibit more stiffness than single-paddled piles for the same plate width. Figure 8 shows that a double-paddled pile exhibited 20–50% more (capacity) efficiency than its corresponding single-paddled pile. In general, the single-paddled pile shows a consistent improvement, as the SPT N value exceeds 5 for the SLS and 10 for the ULS.

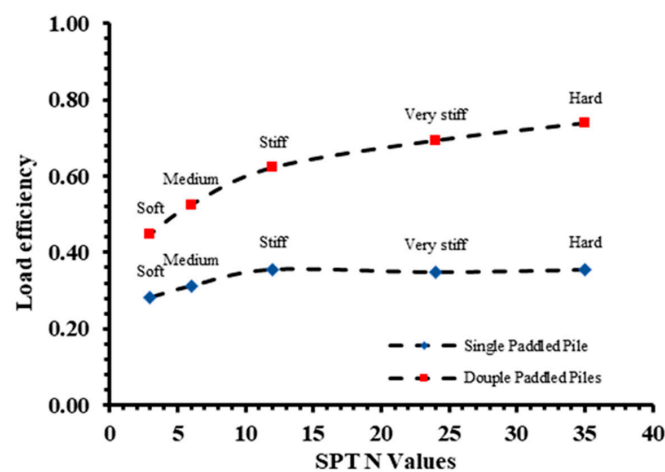
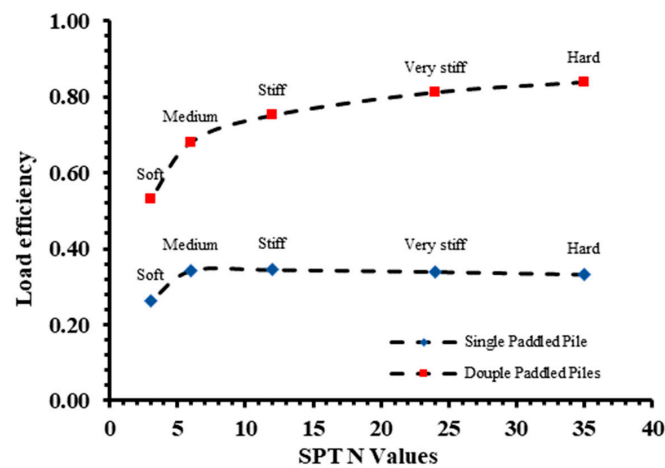


Figure 8. Load efficiency for various SPT N values at lateral deflection: (a) 6.25 mm; (b) 25 mm.

5.2. Effect of Plate Width

This section examines the influence of the plate width on the lateral capacity of single-paddled (SPHP) and double-paddled (DPHP) posts considering [41,44]’s failure criteria. The pile is embedded into a stiff clay soil with the properties shown in Table 5. This study involved varying the plate width in 25% increments, ranging from 0.25 to 2.25 times the original plate width, $W_p = 420$ mm. The lateral capacity primarily depends on the deformation of the soil within the influence zone [34]. The addition of plates increases the surface area of the soil–pile interaction; hence, it involves a greater amount of soil in resisting lateral deflection. Increasing the paddles’ width increases the passive and active soil area for short piles and the passive area for long piles. The soil–pile rigidity criterion proposed by Broms [5] indicates that the pile response is a direct function of the pile width and length. In this study, the obtained results are presented in Figure 9, demonstrating the progressive increase in pile capacity for different plate-to-pile-width ratios for both failure criteria, the SLS and ULS. The calculated maximum lateral load for a double-paddled pile with $W_p/W_f = 1.9$ is 77.0 kN for the SLS and 148.3 kN for the ULS, showing noted improvements of 17% and 15% in the lateral capacity, respectively. For $W_p/W_f = 3.2$, the rate of the increase in lateral capacity declines to 3% for the SLS, 5% for the ULS, and as low as 2% for $W_p/W_f = 4.5$. The lateral capacity of the double-paddled pile is observed, highlighting that it is significantly influenced by the size of the plate, particularly at lower plate-to-pile ratios.

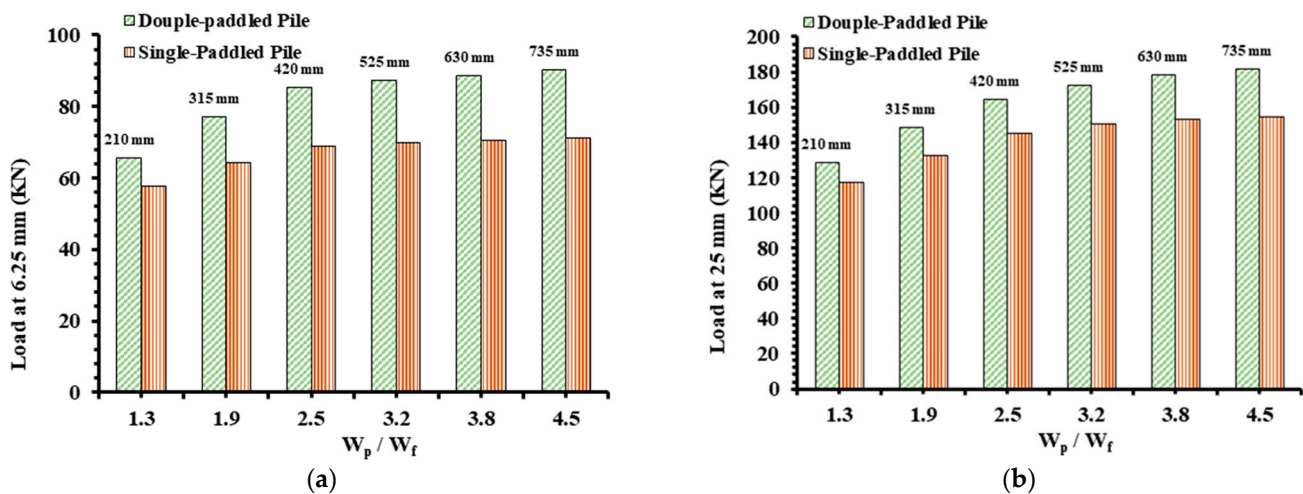


Figure 9. Relationship between lateral load and plate width normalized by pile width: (a) failure criteria of 6.25 mm, SLS; (b) failure criteria of 25 mm, ULS.

The capacity of the single-paddled pile was found to be less affected by the increase in plate width than the DPHP. A plate width equal to 315 mm resulted in an incremental increase in the lateral capacity by 11% for both failure criteria, while a wider (420 mm) plate resulted in a 7% increase. It is evident that as the plate–pile flange width ratio increases, the influence of the plate width on displacement lessens. Figure 9 also demonstrates that when the plate is three times the width of the pile’s flange, the impact of the plate width on the lateral displacement becomes negligible for both double- and single-paddled pile systems. For lateral deflection equal to 6.25 mm (SLS), the lateral load of the double-paddled piles was 13–18.0 kN higher than that of a single-paddled pile for W_p/W_f ratios of 1.3–4.5, indicating that the double-paddled pile is 20% to 26% stiffer than the single-paddled pile, excluding data for $W_p = 250$. In contrast, considering the ULS, the capacity difference between the single-paddled pile and the double-paddled pile is reduced, with the double-paddled pile’s capacity increasing by 12–18 percent.

Figure 10 outlines the load efficiency curve: the correlation between the lateral load efficiency and the width of the plate is observed. It is clear that η_s increases as the plate

width increases; stiffening the pile with one or two plates contributed significantly to the stiffness of the foundation system and provided a 9.0% to 73% increase in rigidity compared to the plain pile. As anticipated, the double-paddled piles demonstrated greater stiffness than single-paddled piles with the same plate width. In general, the SLS study demonstrated a greater load efficiency than the ULS for the same W_p/W_f value, particularly at lower W_p/W_f values. In the ULS analysis, however, greater load efficiency values were estimated for single-paddled piles with $W_p/W_f \geq 2.5$. Figures 9 and 10 reveal that a double-paddled pile exhibited up to 20% for the ULS and 26% for the SLS more stiffness than its corresponding single-paddled pile. This substantial enhancement was attributed to the expanded geometry of the IP, and the soil confinement between the two plates. However, it is expected that the utilization of double plates would incur higher costs. Consequently, single-paddled posts might be a more economically viable option. According to the results shown in Figure 10, the single-paddled pile with $W_p = 420$ ($W_p/W_f = 2.5$) can be considered as the optimal paddle width for IP.

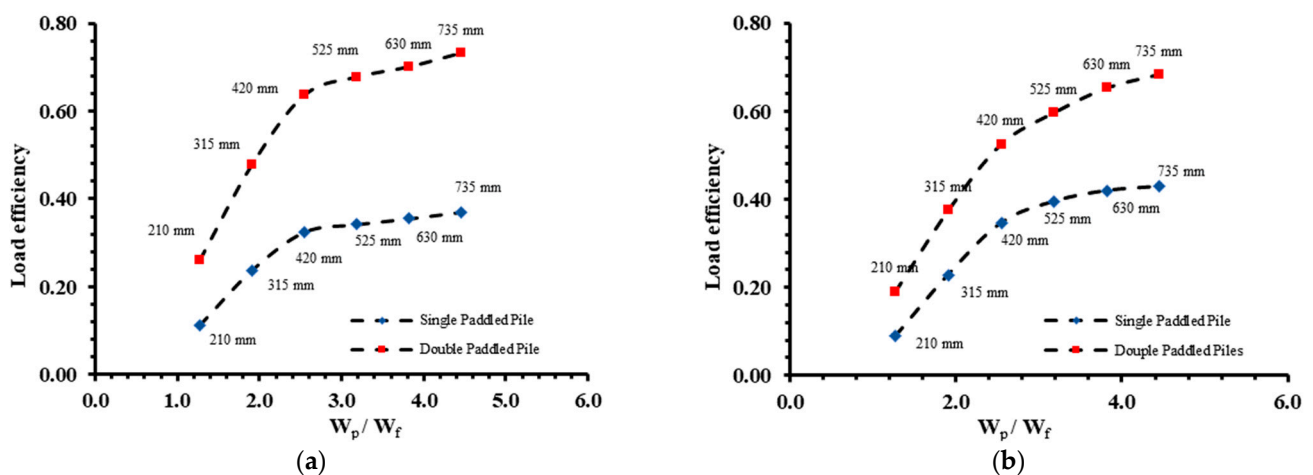


Figure 10. Load efficiency for various W_p/W_f values: (a) SLS; (b) ULS.

Figure 11 illustrates the maximum bending moment fluctuation along the IP shaft and H-pile at a lateral load of 150 KN. The IP bending moment and corresponding H-pile converge together at the bottom of the paddle. The findings have proven that adding plates led to a reduction in the maximum bending moment. Additionally, an increase in the plate width correlated with a decrease in the maximum bending moment. For $W_p/W_f \geq 3.2$, the decrease in the bending moment becomes insignificant. The plate significantly reduces the bending moment in the centre of the H-pile. Furthermore, it was observed that as the plate width increased, the depth at which the maximum bending moment occurred decreased, indicating that the centre of rotation of the pile shifted closer to the ground surface. These findings are consistent with the observations made by [29,30,33,34].

Based on the ULS analysis, the calculated maximum lateral load is 145.3 KN and 164.5 KN for the single- and double-paddled piles with $L_p = 950$ mm, respectively. In general, the lateral load increases as the length of the plate increases. However, the increase in lateral capacity is insignificant (incremental increase $\leq 5\%$) for single-paddled piles with a length-to-width ratio (L/W_p) of 2.8 or greater, as well as for double-paddled piles with an L/W_p of 3.4 or greater, for both the SLS and ULS analysis. According to the ULS, the difference in lateral capacity between the double- and single-paddled piles ranges from 6% to 31% for $L/W_p = 1.1$ and 4.5, respectively, and increases as the ratio increases. A similar overall tendency was seen in the SLS analysis, with greater differential values (18% to 38%) for the same L/W_p ratio.

To optimize the design, load efficiency analyses were performed at different L/W_p values. The double- and single-paddled piles with plate lengths of 0.5 L (475 mm) exhibit a higher capacity than the plain pile by 23% and 16% for the ULS analysis, and 33% and 20%

for the SLS analysis, respectively. Figure 13 shows the load efficiency versus the L/W_p ratio. It is evident that η_s increases as L increases. Considering the ULS, the load efficiency of double-paddled and single-paddled piles with a plate that is 1663 mm long is 87% and 49%, respectively. Regarding the studied configuration, the increase in load efficiency becomes negligible for $L/W_p \geq 2.8$ for a single-paddled pile and $L/W_p \geq 4$ ($L = 1663$ mm) for a double-paddled pile.

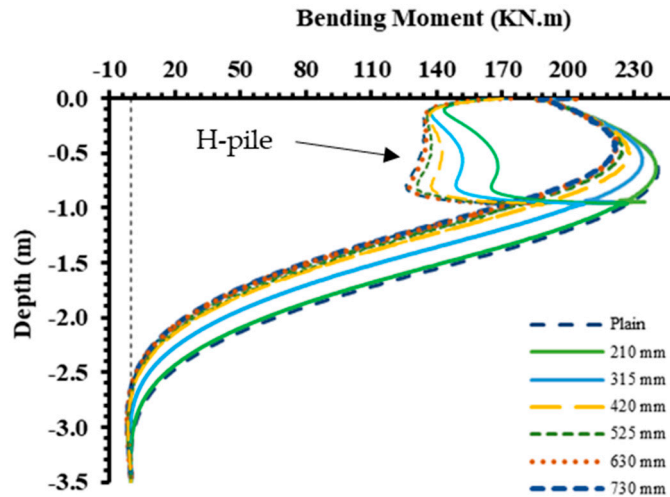


Figure 11. Bending moment versus depth of single-paddled piles with various plate widths.

5.3. Effect of Plate Length

This section evaluates the impact of the plate length on the lateral response of the novel post. The influence of plate length, normalized by its width L/W_p , is illustrated in Figure 12.

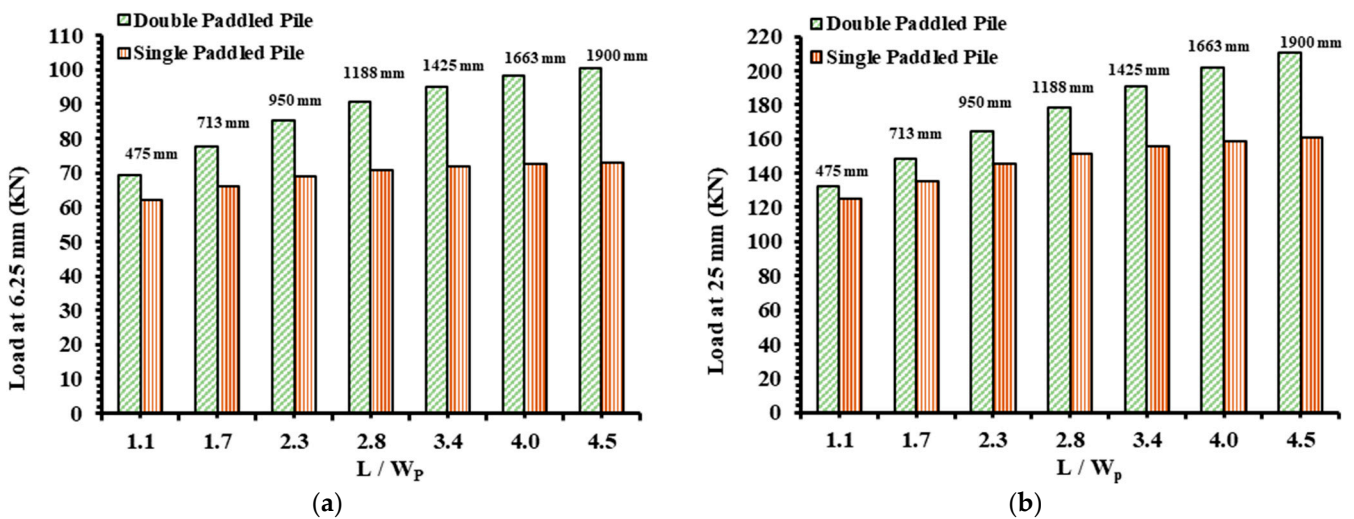


Figure 12. Relationship between lateral deflection and the length of the plate normalized by the width of the pile: (a) SLS; (b) ULS.

The pile flexibility factor, K_r , introduced by [58], offers a means to determine the pile rigidity. This factor takes into account the embedded length-to-diameter ratio (L/D). It is worth noting that the ultimate lateral resistance of the pile is contingent upon its type and configuration. Innovative posts can be categorized as either long piles (flexible) or short piles (rigid), based on the pile length and plates involved. The slenderness ratio, L/D , assumes significance as it serves as a vital indicator of the pile type, specifically the

anticipated failure mode. For long piles, their ultimate lateral resistance is influenced by the pile’s flexural stiffness. As a result, when the maximum applied load is reached, a bending moment equivalent to the pile’s yielding moment is produced. On the other hand, the ultimate lateral resistance of the short piles is governed by soil failure, indicating the force that triggers the failure of the soil mass in front of the pile shaft. In the case of fixed-head short piles, failure is attributed to lateral displacement. Conversely, short piles with free heads fail due to the formation of passive stress on the front side of the upper portion of the pile and active stress below the point of rotation. Assessing the pile stiffness involves examining the embedded length-to-diameter ratio, L/D . Piles with L/D values less than 6 tend to exhibit behaviour akin to short piles, while those with L/D values exceeding 10 are more likely to behave like long piles, as per [16]. Additionally, [59] suggested that flexible piles tend to possess L/D ratios greater than 20.

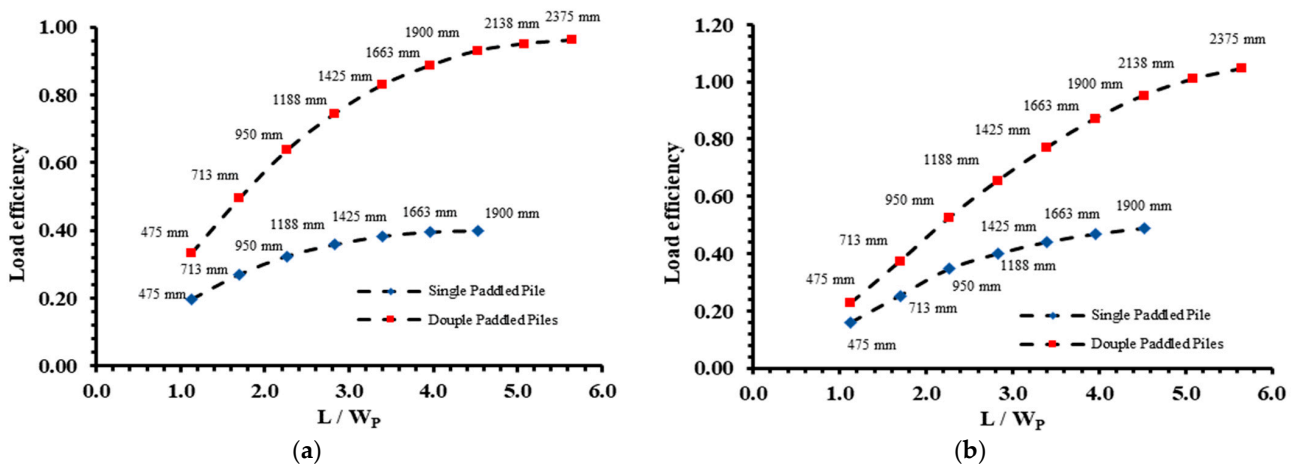


Figure 13. Load efficiency for various L/W_p values: (a) SLS; (b) ULS.

Figure 14 illustrates the lateral displacement profiles of the analyzed systems. In the case of the system where plates are attached to an H-pile with a fixed embedded length of 3.5 m, it exhibited the characteristics of a flexible pile (long pile). The results also indicate that the depth of fixity (i.e., zero lateral deflection and slope) is around -2.8 m and is independent from the width of the plate. Thus, the properties of soil along the top 2.8 have a significant effect on the lateral response of the proposed H-pile. Therefore, an optimal range of plate lengths balances the load-bearing capacity of the post and the width ratio to ensure the efficient design of the innovative post. These results can be used to optimize the design of innovative posts for engineering applications.

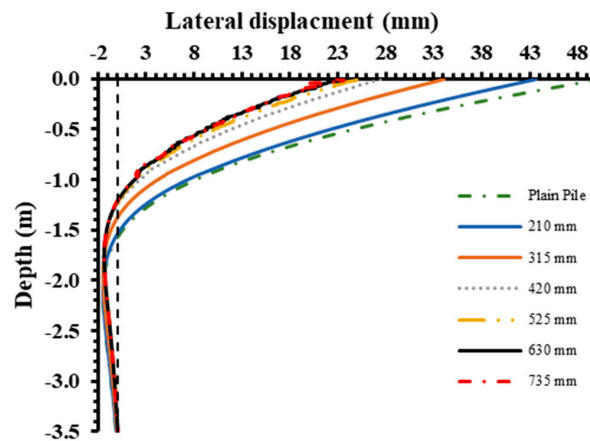


Figure 14. Lateral deflection profile for single-paddled plies, with $L_p = 3.5$ m, $L = 950$ mm, and various plate widths.

5.4. Effect of Plates on the Surrounding Soil

The capacity of laterally loaded piles is governed by the pile rigidity and stiffness and the strength of the surrounding soil. The influence zone of a laterally loaded pile is assumed to be a three-dimensional inverted cone that forms near the ground surface and is centred on the pile [60]. The primary determinant of the pile's lateral resistance is the soil deformation within the influence zone [29].

The average peak shear strength of the tested clay is 97.5 kN/m^2 and the residual shear strength is 16.25 kN/m^2 . Based on the calibrated models for the pile subjected to a lateral load of 50 kN , the induced principal effective stress in the influence zone varies between 28 kN/m^2 and 115 kN/m^2 for SPHPs and DPHPs, and between 28 kN/m^2 and 300 kN/m^2 for PPs. These findings strongly suggest that the soil undergoes plastic deformation, and the zone of plasticity increases as the load increases.

Li et al. [23] showed that the formation of the plastic strain around the pile depends on the displacement and can be divided into four stages. At small displacements, the development of plastic shear strain is not significant. However, as the displacement increases, a plastic shear band emerges near the pile head and extends diagonally downward. Subsequently, with further displacement, a second plastic shear band appears and extends obliquely upward toward the surface, forming a damaging wedge. As the displacement continues to increase, a third plastic shear band forms below the second shear band and exhibits a similar extension toward the surface. Similar stages of the formation of the strain are shown in Figure 15. It is evident that the formation of the plastic zone around the pile will have the same pattern as the strain.

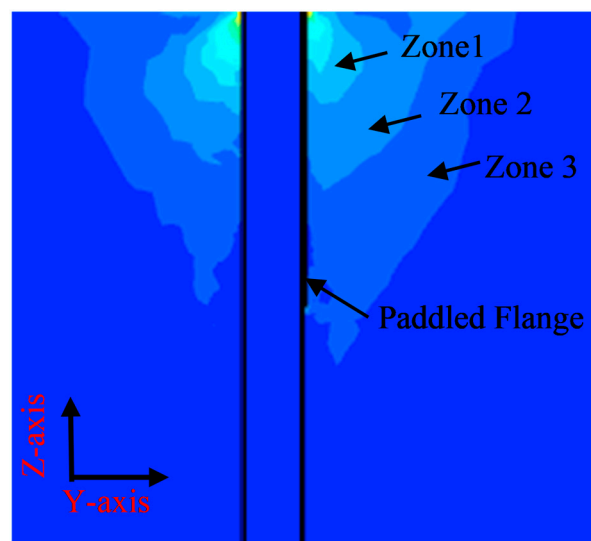


Figure 15. Development process of strain and plastic zone around the pile.

The impact of paddles on the soil–pile interaction can be further elucidated by examining the evolution of the plastic zone within the stiff clay. Previous research has focused on a scenario where winged monopiles are completely embedded into a level soil bed, demonstrating that placing the wings closer to the ground surface enhances the mobilization of soil resistance to lateral pile deflection. This finding has been supported by several studies [33,45,61,62].

The interaction between the paddled piles and soil within the zone of influence is assessed herein. Figure 16 demonstrates the iso-surface plots of the phase shear strain $P\gamma_s$, which provide insight into the extent of the soil influence zone at different W_p values. By adding plates to the flanges of the H-pile, the development of shear strain in the loading direction is reduced in comparison to the conventional H-pile. However, this reduction becomes insignificant as W_p increases, (i.e., $W_p = 525 \text{ mm}$).

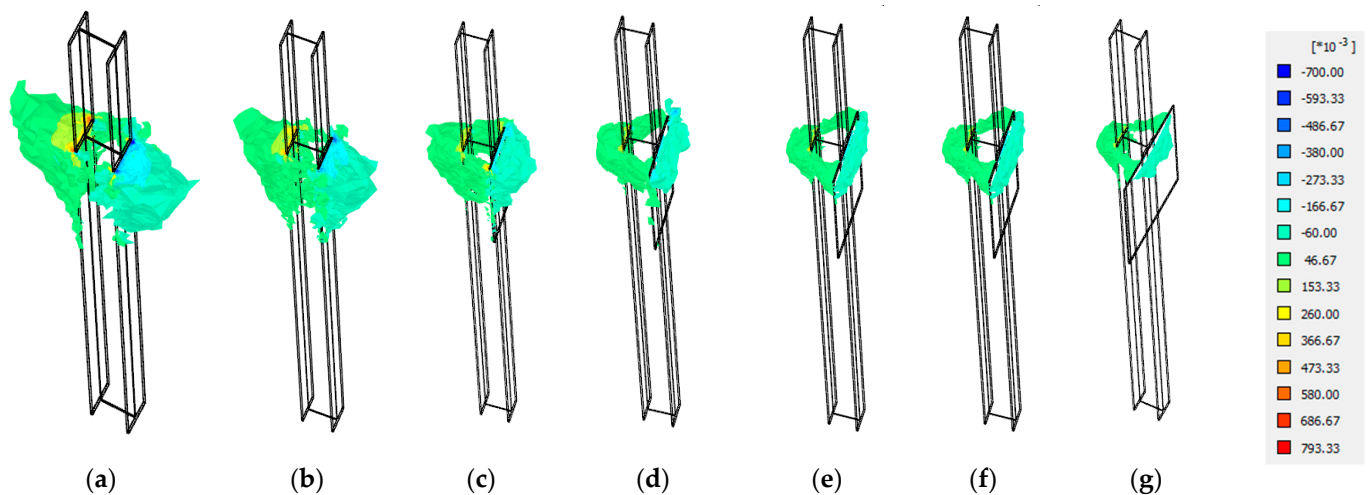


Figure 16. Comparison of phase shear strains of a plain pile and double-paddled piles at different W_p/W_f values: (a) plain pile; (b) $W_p = 210$; (c) $W_p = 315$; (d) $W_p = 420$; (e) $W_p = 525$; (f) $W_p = 630$; (g) $W_p = 735$.

When the plate width is small, such as $W_p/W_f = 210$, the mobilized soil influence zone expands rapidly and covers the entire plate width. This means that the entire paddle plays a role in mobilizing the soil resistance. In contrast, for W_p values greater than or equal to 525 mm, the development of the mobilized soil influence zone is slower. In this scenario, the contribution of the plate to the lateral load resistance is minimal, and a portion of it lies outside the mobilized influence zone.

6. Conclusions

This investigation focuses on evaluating the performance of innovative posts proposed for supporting structures subjected to lateral loads (i.e., sound walls). The innovative post design consists of a single or double plate attached to the flanges of a steel H-pile, and its lateral behaviour in cohesion (clay) soil is simulated using finite element (FE) models developed using the PLAXIS 3D software. The comparison between the numerical model predictions and field load test results demonstrates a favourable agreement, validating the capability of the developed numerical models to simulate the lateral response of the innovative posts. The validated model was used to assess the response of the IP considering different configurations and clay consistencies. The lateral capacity of the IP decreases as the S_u value decreases; however, the rate of change differed slightly depending on the failure criteria.

6.1. Findings

Based on an experimental investigation and finite element analysis of single- and double-paddled H-piles in clay, the following conclusions were drawn.

6.2. Number of Plates

The double-paddled pile exhibited significantly higher stiffness, up to 25% for the ultimate limit state (ULS) and 35% for the serviceability limit state (SLS), compared to its corresponding single-paddled pile. However, it is worth noting that the utilization of double plates is expected to come with higher costs. Therefore, from an economic standpoint, single-paddled posts may represent a more financially viable option.

6.3. Plate Width

1. The capacity of the single-paddled pile was found to be less affected than the double-paddled pile by the increase in plate width.

2. When the plate width \geq three times the width of the pile's flange, the impact of the plate width on the lateral displacement becomes negligible for both double-paddled and single-paddled pile systems.

3. Increasing the plate width led to a corresponding increase in η_s , indicating enhanced stiffness. The inclusion of one or two plates significantly contributed to the overall rigidity of the foundation system, resulting in a substantial 9.0% to 73% increase in stiffness compared to a plain pile.

4. The addition of plates reduces the maximum bending moment in the foundation and in the centre of the H-pile, with a further decrease observed as the plate width increases.

6.4. Plate Length

1. As the plate length increases, the lateral load capacity increases. However, the increase in the lateral capacity is negligible for single-paddled piles with a length-to-width ratio (L/W_p) of 2.8 or greater, as well as for double-paddled piles with an L/W_p of 3.4 or greater.

2. The load efficiency increases with the increase in the plate length, but becomes negligible for $L/W_p \geq 2.8$, for single-paddled piles and $L/W_p \geq 4$ double-paddled piles.

6.5. Effect on the Surrounding Soil

The development of shear strain in the loading direction is reduced for paddled piles in comparison to plain H-piles. However, this reduction becomes insignificant for $W_p \geq 525$ mm. For smaller values of W_p/W_f (plate-width-to-flange-width ratio), the mobilized soil influence zone expands at a faster rate.

6.6. Future Recommendations

It is recommended that future research extends the scope to evaluate the dynamic behaviour of sound walls subjected to wind loading, considering potential resonant frequencies and the damping characteristics of the piles. This additional analysis could provide valuable insights into the structural response under dynamic wind conditions, enhancing the overall understanding of the system's performance.

As a further suggestion for future work, it is recommended to explore the impact of combined load conditions involving both vertical and lateral forces on PHPs. Investigating the structural response under such combined loading scenarios would contribute valuable insights into the comprehensive behaviour of the system.

Author Contributions: A.A.: Conceptualization, data curation, formal analysis, investigation, methodology, software, validation, visualization, writing—original draft. M.H.E.N.: Conceptualization, funding acquisition, project administration, resources, methodology, supervision, writing—review and editing. All authors have read and agreed to the published version of the manuscript.

Funding: I would like to thank Mitacs Accelerate Program for funding this research project, grant number IT29511.

Data Availability Statement: All data and materials are available on request from the corresponding author. The data are not publicly available due to ongoing research using a part of the data.

Acknowledgments: I begin by praising the Almighty: Praise be to Allah, Lord of all creation, the Source of all wisdom and enlightenment. I thank Allah for guiding and helping me through this journey of learning, and I ask Allah to forgive my shortcomings. Peace and blessings be upon the noble messenger, Prophet Muhammad, who emphasized the value of learning and perfecting the work by stating that Allah, most High, loves for you to perfect an act when you perform it. Additionally, he (SAWS) emphasized the value of gratitude by stating that one who does not thank people does not thank Allah. In this realm of gratitude, I would like to acknowledge Atlantic Industries Limited and in particular Dereck Essery for their support and positive feedback on the work.

Conflicts of Interest: The funders had no role in the design of the study; in the collection, analyses, or interpretation of data; in the writing of the manuscript; or in the decision to publish the results.

References

1. Long, J.H.; Vanneste, G. Effects of cyclic lateral loads on piles in sand. *J. Geotech. Eng.* **1994**, *120*, 225–244. [[CrossRef](#)]
2. Fleming, K.; Weltman, A.; Randolph, M.; Elson, K. Piling Engineering. In *Piling Engineering*; CRC Press: Boca Raton, FL, USA, 2008. [[CrossRef](#)]
3. Matlock, H.; Reese, L.C. Generalized Solutions for Laterally Loaded Piles. *J. Soil Mech. Found. Div.* **1960**, *86*, 63–92. [[CrossRef](#)]
4. Davisson, M. Lateral load capacity of piles. In Proceedings of the 49th Annual Meeting of the Highway Research Board, Washington, DC, USA, 12–16 January 1970.
5. Broms, B.B. Lateral Resistance of Piles in Cohesive Soils. *J. Soil Mech. Found. Div.* **1964**, *90*, 27–63. [[CrossRef](#)]
6. Matlock, H. Correlation for Design of Laterally Loaded Piles in Soft Clay. In Proceedings of the Annual Offshore Technology Conference, Houston, TX, USA, 22–24 April 1970. [[CrossRef](#)]
7. Reese, L.C.; Cox, W.R.; Koop, F.D. Analysis of Laterally Loaded Piles in Sand. In Proceedings of the Annual Offshore Technology Conference, Houston, TX, USA, 6–8 May 1974; pp. 473–480. [[CrossRef](#)]
8. Winkler, E. *The Teaching of Elasticity and Strength with Special Regard to Their Application in Technology for Polytechnic Schools, Construction Academies, Engineers, Mechanical Engineers, Architects*; Dominicus, H., Ed.; 1867.
9. Das, B.M.; Sivakugan, N. *Fundamentals of Geotechnical Engineering*; Cengage Learning: Boston, MA, USA, 2018.
10. Khodair, Y.; Abdel-Mohti, A. Numerical Analysis of Pile–Soil Interaction under Axial and Lateral Loads. *Int. J. Concr. Struct. Mater* **2014**, *8*, 239–249. [[CrossRef](#)]
11. Fahmy, A.; El Naggar, M.H. Cyclic lateral performance of helical tapered piles in silty sand. *DFI J.—J. Deep. Found. Inst.* **2016**, *10*, 111–124. [[CrossRef](#)]
12. Wang, H.; Lehane, B.M.; Bransby, M.F.; Wang, L.Z.; Hong, Y. Field and numerical study of the lateral response of rigid piles in sand. *Acta Geotech.* **2022**, *17*, 5573–5584. [[CrossRef](#)]
13. Consoli, N.C.; Diambra, A.; Cordeiro, R.E.; Born, R.B.; Cheng, X. Field and Numerical Analysis of Cyclic Displacement Controlled Lateral Load Tests on Driven Piles in a Residual Soil. *Geotech. Geol. Eng.* **2023**, *41*, 685–705. [[CrossRef](#)]
14. Eltaweila, S.; Shahien, M.M.; Nasr, A.M.; Farouk, A. Effect of Soil Improvement Techniques on Increasing the Lateral Resistance of Single Piles in Soft Clay (Numerical Investigation). *Geotech. Geol. Eng.* **2021**, *39*, 4059–4070. [[CrossRef](#)]
15. Shi, Z.; Liu, L.; Huang, M.; Shen, K.; Wang, B. Simulation of cyclic laterally-loaded piles in undrained clays accounting for soil small-strain characteristics. *Ocean Eng.* **2023**, *267*, 113268. [[CrossRef](#)]
16. Tomlinson, M.; Woodward, J. *Pile Design and Construction Practice*, 6th ed.; CRC Press: Boca Raton, FL, USA, 2015; pp. 1–575. Available online: <https://menglim498.files.wordpress.com/2013/04/pile-design-and-construction.pdf> (accessed on 26 February 2023).
17. Tsetas, A.; Gómez, S.S.; Tsouvalas, A.; van Beek, K.; Tehrani, F.S.; Kementzetzidis, E.; Pisano, F.; Elkadi, A.; Segeren, M.; Molenkamp, T.; et al. Experimental identification of the dynamic behaviour of pile-soil system installed by means of three different pile-driving techniques. In Proceedings of the XI International Conference on Structural Dynamics, Athens, Greece, 23–26 November 2020; pp. 3005–3015. [[CrossRef](#)]
18. Mroz, D.; El Naggar, M.H.; Director, R.; El Sharnouby, M.; Essery, D. Experimental and Numerical Evaluation of Plate Modified H-Piles Subjected to Monotonic and Cyclic Lateral Loading. TAC Conference & Exhibition. 2020. Available online: https://www.tac-atc.ca/sites/default/files/conf_papers/elnaggarh-evaluation_of_modified_h-piles_subject_to_lateral.pdf (accessed on 16 May 2022).
19. Achmus, M.; Schmoor, K.A.; Herwig, V.; Matlock, B. Lateral bearing behaviour of vibro- and impact-driven large-diameter piles in dense sand. *Geotechnik* **2020**, *43*, 147–159. [[CrossRef](#)]
20. Stein, P.; Gattermann, J.; Daumlechner, E.; Hinzmann, N.; Stahlmann, J. *Großmaßstäbliche Modellversuche zur Lateralen Tragfähigkeit Offener Stahlrohrpfähle unter Zyklischer Belastung bei Verschiedenen Einbringungsverfahren: Forschungsvorhaben ZykLaMP (Zyklisch-Lateral-Monopile)*; Technische Universität Braunschweig, Institut für Geomechanik und Geotechnik: Braunschweig, Germany, 2020.
21. Labenski, J.; Moormann, C. Lateral bearing behaviour of vibratory-driven monopiles: A modified p-y approach based on experimental observations of scaled model tests. In Proceedings of the 17th European Conference on Soil Mechanics and Geotechnical Engineering, ECSMGE 2019, Reykjavik, Iceland, 1–6 September 2019. [[CrossRef](#)]
22. Mroz, D. Experimental and Numerical Evaluation of a Novel Piling System for Sound Wall Applications. Ph.D. Thesis, The University of Western Ontario, London, ON, Canada, September 2019. Available online: <https://ir.lib.uwo.ca/etd/6563> (accessed on 24 November 2023).
23. Li, L.; Zheng, M.; Liu, X.; Wu, W.; Liu, H.; El Naggar, M.H.; Jiang, G. Numerical analysis of the cyclic loading behavior of monopile and hybrid pile foundation. *Comput. Geotech.* **2022**, *144*, 104635. [[CrossRef](#)]
24. Li, L.; Liu, X.; Liu, H.; Wu, W.; Lehane, B.M.; Jiang, G.; Xu, M. Experimental and numerical study on the static lateral performance of monopile and hybrid pile foundation. *Ocean Eng.* **2022**, *255*, 111461. [[CrossRef](#)]
25. Dührkap, J.; Grabe, J. Laterally loaded piles with bulge. *J. Offshore Mech. Arct. Eng.* **2008**, *130*, 041602. [[CrossRef](#)]
26. Murphy, G.; Doherty, P.; Cadogan, D.; Gavin, K. Field experiments on instrumented winged monopiles. *Proc. Inst. Civ. Eng.-Geotech. Eng.* **2016**, *169*, 227–239. [[CrossRef](#)]
27. Grabe, J.; Dührkop, J. Improving of lateral bearing capacity of mono-piles by welded wings. In *Proceedings of the 2nd International Conference on Foundations*; HIS BRE Press: Garston, UK, 2007.

28. Bienen, B.; Dührkop, J.; Grabe, J.; Randolph, M.F.; White, D.J. Response of Piles with Wings to Monotonic and Cyclic Lateral Loading in Sand. *J. Geotech. Geoenviron. Eng.* **2011**, *138*, 364–375. [[CrossRef](#)]
29. Nasr, A.M.A. Experimental and theoretical studies of laterally loaded finned piles in sand. *Can. Geotech. J.* **2013**, *51*, 381–393. [[CrossRef](#)]
30. Odhambo, A.K. Model Study of the Static and Cyclic Lateral Capacity of Finned Piles. Available online: [https://preserve.lib.lehigh.edu/islandora/object/preserve:bp-13881540?solr_nav\[id\]=2e0c145d4fb03c4f4215&solr_nav\[page\]=0&solr_nav\[offset\]=1](https://preserve.lib.lehigh.edu/islandora/object/preserve:bp-13881540?solr_nav[id]=2e0c145d4fb03c4f4215&solr_nav[page]=0&solr_nav[offset]=1) (accessed on 23 November 2023).
31. Dührkop, J. Zum Einfluss von Aufweitungen und Zyklischen Lasten auf das Verformungsverhalten Lateral Beanspruchter Pfähle in Sand—Deutsche Digitale Bibliothek. TUHH. Available online: <https://www.deutsche-digitale-bibliothek.de/item/6L6SRD3H6EWOS56AZIPAZBDP2TW5HYX3> (accessed on 23 November 2023).
32. Lutenecker, A.J. Tension Tests on Driven Fin Piles for Support of Solar Panel Arrays. In Proceedings of the GeoCongress 2012: State of the Art and Practice in Geotechnical Engineering, Oakland, CA, USA, 25–29 March 2012; pp. 305–314. [[CrossRef](#)]
33. Babu, K.V.; Viswanadham, B.V.S. Numerical studies on lateral load response of fin piles. *Geomech. Geoengin.* **2019**, *14*, 85–98. [[CrossRef](#)]
34. Pei, T.; Qiu, T. A Numerical Investigation of Laterally Loaded Steel Fin Pile Foundation in Sand. *Int. J. Geomech.* **2022**, *22*, 04022102. [[CrossRef](#)]
35. Drbe, O. Investigation of Hollow Bar Micropiles in Cohesive Soil. Ph.D. Thesis, The University of Western Ontario, London, ON, Canada, December 2013. Available online: <https://ir.lib.uwo.ca/etd/1770> (accessed on 24 November 2023).
36. Yehia, A.; Elaziz, A. *Performance of Hollow Bar Micropiles under Axial and Lateral Loads in Cohesive Soils (Spine Title: Performance of Hollow Bar Micropiles under Different Loads)*; The University of Western Ontario: London, ON, Canada, 2012.
37. ASTM D3689; Standard Test Methods for Deep Foundations Under Lateral Load. ASTM: West Conshohocken, PA, USA, 2013. Available online: https://www.astm.org/d3966_d3966m-07r13e01.html (accessed on 11 October 2023).
38. Guo, P.X.; Xiao, Y.; Kunnath, S.K. Performance of laterally loaded H-piles in sand. *Soil Dyn. Earthq. Eng.* **2014**, *67*, 316–325. [[CrossRef](#)]
39. Hansen, J.B. A General Formula for Bearing Capacity. 1961. Available online: <https://api.semanticscholar.org/CorpusID:18917091> (accessed on 11 March 2022).
40. Das, S. *Functional Fractional Calculus*; Springer: Berlin, Germany, 2011. [[CrossRef](#)]
41. McAulity, J.F.M. Thrust Loading on Piles. *J. Soil Mech. Found. Div.* **1956**, *82*, 1–25. [[CrossRef](#)]
42. Walker, J.; Cox, E.H. Design of Pier Foundations for Lateral Loads. *Trans. ASABE* **1966**, *9*, 0417–0420. [[CrossRef](#)]
43. Nusairat, J.; Liang, R.Y.; Engel, R.; Hanneman, D.; Abu-Hejleh, N.; Yang, K. Drilled Shaft Design for Sound Barrier Walls, Signs, and Signals. 2004. Available online: <https://www.codot.gov/programs/research/pdfs/2004/drilledshaft.pdf> (accessed on 10 December 2022).
44. Building Code of the City of New York. Available online: <https://www.nyc.gov/site/buildings/codes/nyc-code.page> (accessed on 23 November 2023).
45. Peng, J.R.; Rouainia, M.; Clarke, B.G. Finite element analysis of laterally loaded fin piles. *Comput. Struct.* **2010**, *88*, 1239–1247. [[CrossRef](#)]
46. Kulhawy, F.; Mayne, P. *Manual on Estimating Soil Properties for Foundation Design*; Electric Power Research Institute: Palo Alto, CA, USA; Cornell University: Ithaca, NY, USA, 1990.
47. Flaate, K. Effects of Pile Driving in Clays. *Can. Geotech. J.* **2011**, *9*, 81–88. [[CrossRef](#)]
48. Randolph, M.F.; Carter, J.P.; Wroth, C.P. Driven piles in clay—The effects of installation and subsequent consolidation. *Géotechnique* **2015**, *29*, 361–393. [[CrossRef](#)]
49. Stroud, M. *The Standard Penetration Test in Insensitive Clays and Soft Rocks*, 2nd ed.; John Wiley: New York, NY, USA, 1975.
50. Sivrikaya, O.; Toğrol, E. Determination of undrained strength of fine-grained soils by means of SPT and its application in Turkey. *Eng. Geol.* **2006**, *86*, 52–69. [[CrossRef](#)]
51. Terzaghi, K.; Peck, R.B.; Mesri, G. *Soil Mechanics in Engineering Practice*, 3rd ed.; John Wiley & Sons: Hoboken, NJ, USA, 1996.
52. Kumar, R.; Bhargava, K.; Choudhury, D. Estimation of Engineering Properties of Soils from Field SPT Using Random Number Generation. *INAE Lett.* **2016**, *1*, 77–84. [[CrossRef](#)]
53. NRC National Building Code of Canada. 2005. Available online: <https://nrc-publications.canada.ca/eng/view/object/?id=2623b771-c768-4b67-a2df-0d5895011263> (accessed on 12 April 2023).
54. Bjerrum, L.; Anderson, K.H. *In-Situ Measurement of Lateral Pressures in Clay*; Norwegian Geotechnical Institute Publ.: Oslo, Norway, 1972.
55. Bowles, J.E. *Foundation Analysis and Design*, 5th ed. The McGraw-Hill Companies: New York, NY, USA; St. Louis, MO, USA; San Francisco, CA, USA, 1996.
56. Sivrikaya, O.; Ergün, T. Relationships between SPT-N value and undrained shear strength of fine-grained soils in Turkey. *Tek. Dergi* **2007**, *18*, 4229–4246.
57. Karol, R. *Soils and Soil Engineering*; Prentice Hall: Hoboken, NJ, USA, 1960; Available online: <https://trid.trb.org/view/521681> (accessed on 12 August 2023).
58. Poulos, H.; Davis, E. *Pile Foundation Analysis and Design*; Wiley: New York, NY, USA, 1980.

-
59. Kasch, V.R.; Coyle, H.; Bartoskewitz, R.E.; Sarver, W.G. Lateral Load Test of a Drilled Shaft in Clay. 1977. Available online: <https://trid.trb.org/view/75872> (accessed on 3 January 2023).
 60. Murff, J.D.; Hamilton, J.M. PUltimate for Undrained Analysis of Laterally Loaded Piles. *J. Geotech. Eng.* **1993**, *119*, 91–107. [[CrossRef](#)]
 61. Abongo, K.O. Model study of the static and cyclic lateral capacity of finned piles. Ph.D. Thesis, Lehigh University, Bethlehem, PA, USA, 2019.
 62. Peng, J.-R. Behaviour of Finned Piles in Sand under Lateral Loading. Ph.D. Thesis, Newcastle University, Newcastle, UK, 2006.

Disclaimer/Publisher’s Note: The statements, opinions and data contained in all publications are solely those of the individual author(s) and contributor(s) and not of MDPI and/or the editor(s). MDPI and/or the editor(s) disclaim responsibility for any injury to people or property resulting from any ideas, methods, instructions or products referred to in the content.